J Biol Inorg Chem (2014) 19:659–666
DOI 10.1007/s00775-014-1130-9

ORIGINAL PAPER

Solid-state NMR studies of metal-free SOD1 fibrillar structures

Lucia Banci · Olga Blaževitš · Francesca Cantini · Jens Danielsson · Lisa Lang · Claudio Luchinat · Jiafei Mao · Mikael Oliveberg · Enrico Ravera

Received: 20 November 2013 / Accepted: 10 March 2014 / Published online: 10 April 2014

Abstract Copper–zinc superoxide dismutase 1 (SOD1) is present in the protein aggregates deposited in motor neurons of amyotrophic lateral sclerosis (ALS) patients. ALS is a neurodegenerative disease that can be either sporadic (ca. 90 %) or familial (fALS). The most widely studied forms of fALS are caused by mutations in the sequence of SOD1. Ex mortuo SOD1 aggregates are usually found to be amorphous. In vitro SOD1, in its immature reduced and apo state, forms fibrillar aggregates. Previous literature data have suggested that a monomeric SOD1 construct, lacking loops IV and VII, (apoSODΔIV–VII), shares the same fibrillization properties of apoSOD1, both proteins having the common structural feature of the central β-barrel. In this work, we show that structural information can be obtained at a site-specific level from solid-state NMR. The residues that are sequentially assignable are found to be located at the putative nucleation site for fibrillar species formation in apoSOD, as detected by other experimental techniques.

Keywords Copper–zinc superoxide dismutase 1 · SOD1 · Solid-state NMR · Fibrils · Aggregation · ALS

Introduction

Protein misfolding often leads to the formation, and subsequent deposition, of insoluble protein aggregates. Although in few cases such depositions may play a physiological role [1], in the majority of cases they are associated with neurodegenerative diseases [2, 3]. Among these, amyotrophic lateral sclerosis (ALS) symptoms is a fatal adult-onset neurodegenerative disease characterized by the progressive dysfunction and loss of motor neurons. More than 90 % of ALS incidences are of unknown cause and are termed sporadic (sALS). The remaining ALS cases show familial inheritance (fALS) and are caused by

Responsible Editors: Lucia Banci and Claudio Luchinat.

Electronic supplementary material The online version of this article (doi:10.1007/s00775-014-1130-9) contains supplementary material, which is available to authorized users.

L. Banci (✉) · O. Blaževitš · F. Cantini · C. Luchinat (✉) · J. Mao · E. Ravera
Magnetic Resonance Center (CERM), University of Florence, Via L. Sacconi 6, 50019 Sesto Fiorentino, Italy
e-mail: banci@cerm.unifi.it

C. Luchinat
e-mail: luchinat@cerm.unifi.it

L. Banci · F. Cantini · C. Luchinat · E. Ravera
Department of Chemistry, University of Florence, Via della Lastruccia 3, 50019 Sesto Fiorentino, Italy

L. Banci · C. Luchinat · J. Mao
Fondazione Farmacogenomica FiorGen onlus, Via L. Sacconi 6, 50019 Sesto Fiorentino, Italy

J. Danielsson · L. Lang · M. Oliveberg
Arrhenius Laboratories of Natural Sciences, Department of Biochemistry and Biophysics, Stockholm University, 106 91 Stockholm, Sweden

Present Address:
J. Mao
Goethe Universität, Max-von-Laue-Strasse 9, Biozentrum N202, 60438 Frankfurt am Main, Germany

mutations in a number of genes in a dominant manner. The most thoroughly studied forms of fALS are caused by mutations in the gene encoding human copper–zinc superoxide dismutase (SOD1), accounting for 10–15 % of all fALS cases [4–6]. Intracellular proteinaceous depositions have been found in spinal cords from fALS-SOD1 patients and in model mice developing ALS [7–11]. Post-mortem studies carried out on ALS patients' motor neurons showed the presence of amorphous Lewy body-like hyaline inclusion bodies composed of 15- to 25-nm granule-coated fibrils that are immunoreactive to SOD1 [12] while both filamentous and amorphous aggregates constitute the pathological inclusions in the transgenic mice.

It has been reported that even immature wild-type SOD1 (WT SOD1) aggregates [13, 14], though a number of pathogenic mutations increases its propensity for insoluble aggregation [15]. Insoluble aggregates are often associated to mitochondria [16, 17].

SOD1 is a 32-kDa homodimeric enzyme which binds one copper and one zinc ion per monomer and contains an intrasubunit Cys57–Cys146 disulfide bond. These post-translational modifications of SOD1 contribute greatly to the stability of the enzyme. The fully mature, dimeric and metallated protein (Cu_2,Zn_2-$SOD1_{2SS}$) is indeed one of the most stable enzymes known, with a melting temperature of around 90 °C [18–20] and no tendency to aggregate in physiological conditions. Removal of the metal ions leads to a dramatic loss of protein stability (the melting temperature decreases to 52 °C and to the propensity to aggregate [21–23].

Three possible mechanisms are usually considered when analyzing apoSOD1 aggregation, namely

(a) oxidative cross-linking via inter-molecular cysteine residues [24];
(b) assembly via the flexible loop bearing the zinc active site [25, 26];
(c) reassembly of segments after rupturing of the central β-barrel [27, 28].

The structural and dynamical characterization of the apo state of SOD1 and some of its fALS mutants showed that in solution apo SOD1 is highly disordered, sampling a large range of conformations [29]. This explains why only the disordered, locally unfolded, metal-free state is prone to oligomerize under physiological conditions, whereas the rigid structure of the metalated protein is unable to do it [13]. The disulfide bond reduction of the demetallated protein further destabilizes the protein and leads to the loss of its quaternary structure [30–32] and the monomeric species itself could constitute the seed for SOD1 aggregation [23, 33]. Moreover, it has been shown that a small amount of disulfide-reduced apo SOD1 is able to induce the aggregation of more stable, disulfide-intact SOD1 dimers [22]. Some of us previously investigated, using solid-state NMR (SSNMR), the role of the flexible loops bearing the metal-coordination site, finding evidence for an increased beta-structure content of the loops IV and VII in the "fibril ready state" of the apoprotein in solution with respect to the apoprotein microcrystals [34].

Some of us have also recently reported that constructs of the apo protein lacking the disulfide bond, the flexible loops IV and VII, or both, share highly similar fibrillation properties, concluding that as the central β-barrel is the only common structural motif of the three constructs it should therefore contain the aggregation core [35]. Studies based on limited proteolysis also suggested that the fibrils of SOD1 consist of a fibrillar core that is coated with disordered, solvent-accessible protein stretches [36]. In the present work, we report an atomic-level characterization of SOD1 fibrillar aggregates by SSNMR with the goal of understanding the nucleation site of the aggregation. No attempts on high-resolution characterization of SOD1 fibrils have been reported so far [36] while SSNMR has been successfully applied over the years to the structural characterization of protein fibrils, oligomeric species and aggregates [37–53], as well as to the study of complex protein–biomineral systems [54–57].

To avoid the contribution of the solvent-accessible protein stretches to the spectrum, we selected a simpler construct lacking the disulfide bond and the flexible loops IV and VII [58], which maintains some aggregation properties as of WT apoSOD1 [35]. In this construct (apo-SODΔIV–VII), residues 49–81 (loop IV, connecting the strands 4 and 5) and 124–139 (loop VII, connecting the strands 7 and 8) were replaced with short Gly-Ala-Gly tripeptide linkers. As a result of loop IV removal, a significant portion of the dimer interface, including Phe-50 and Gly-51 as well as Cys-57 involved in the disulfide bond with Cys-146, is disrupted, thus producing a monomeric apo protein. Further, the remaining free cysteines were also removed by the mutations C6A/C111S/C146S. In this way we simplified a system otherwise very challenging to study in its physiological state, which gives rise mainly to amorphous form. This is consistent with the observation that aggregates ex mortuo are usually found to be amorphous material containing SOD1 protein together with other proteins [12]. This study on a simplified system could therefore capture the essence of the initial steps of the pathological aggregation mechanism and could play a key role in our understanding of such mechanism.

In this communication, for the first time we reveal some structural features of complex SOD1 fibrils by taking advantage of high-field high-resolution magic-angle spinning (MAS) SSNMR and by partially alleviating spectral overlap through a functionally simplified protein (apo-SODΔIV–VII).

Materials and methods

NMR samples preparation

Plasmid of SODΔIV–VII construct and WT SOD1 were transformed into *Escherichia coli* Origami pLysS strain by heat shock. The cells were grown in M9 minimal medium supplemented with 100 μg/mL carbenicillin, 1 g/L $^{15}(NH_4)_2SO4$, and 3 g/L $^{13}C_6$ glucose at 37 °C. When OD reached 0.7, the cultures were induced using 0.5 mM IPTG over night at 25 °C. The next day cells were harvested by centrifugation at 7,400 rpm in a Beckman Avanti J-20 centrifuge, JLA 8.1000 rotor, followed by resuspension of the cells in 50 mM Tris–HCl, pH 7.5. All purification steps were performed at +4 °C. Cell were lysed by ultrasonication and centrifuged at 15,000 rpm. The supernatant was subjected to 50 % $(NH_4)_2SO_4$ precipitation. After centrifugation at 18,000 rpm and additional $(NH_4)_2SO_4$ precipitation at 90 %, saturation SODΔIV–VII was recovered from the pellet after centrifugation at 18,000 rpm by resuspension in 50 mM Tris–HCl, pH 7.5. Residual $(NH_4)_2SO_4$ was removed by dialysis against 10 mM Tris–HCl, pH 7.5 over night. Next, the supernatant was loaded to a Q-Sepharose anion-exchange column (Amersham Bioscience). The protein was eluted by a linear 0–1 M NaCl gradient in 50 mM Tris–HCl, pH 7.5, and purity analyzed using 15 % SDS PAGE. The fractions were collected and dialyzed against milliQ H_2O and centrifuged at 18,000 rpm and stored at −20 °C.

Some kind of stimulus is required to prompt the aggregation of proteins [35]. One of these stimuli is mechanical agitation, as achieved by stirring or shaking of the sample [39, 53, 59, 60]. As far from physiology as this may seem, such experiments are crucial to elucidate the key steps of pathological aggregation.

SODΔIV–VII fibrils were prepared as described by [35] diluting freshly prepared ^{13}C-^{15}N SODΔIV–VII at 200–230 μM concentration in 10 mM Bis–Tris, pH 6.2 up to the final volume of 10 mL. The obtained solution was incubated at 37 °C for 4 days with shaking at 1,200 rpm to get well-matured fibrils.

WT SOD1 fibrils were obtained from freshly prepared ^{13}C-^{15}N apo SOD1 at the concentration of 50 μM in 20 mM sodium phosphate, pH 7.4, 100 mM NaCl with the addition of 1 M GdmHCl and 1 mM EDTA was incubated at a final volume of 1 mL in 2-mL glass vials containing 3 Teflon balls and agitated at 950 rpm for 3–4 weeks. All solutions were filtered through a 0.22-μm syringe filter prior to use.

The fibrils were collected by ultracentrifugation at 60,000 rpm in 70Ti Beckman coulter rotor for 48 h at 4 °C. The pellet was washed with fresh, cold ultrapure water (Millipore) 3 times (1 mL each time), and then approximately 10 mg of wet material was packed into a Bruker 3.2-mm zirconia rotor. The fibril samples were kept fully hydrated during all steps.

All the SSNMR spectra were recorded on Bruker Avance 850 and 700 MHz wide-bore instruments operating at 20.0 and at 16.4 T, respectively. The effective sample temperature was stabilized at 288 K for all solution and at 265 K at stator outlet for solid-state NMR experiments. The MAS frequency was set to 14 kHz and a ^{1}H SWTPPM decoupling of 75 kHz was applied in all the evolution delays. Standard pulse sequences were used for the set of SSNMR spectra (2D DARR [61], 2D NCA/NCO [62, 63], 3D NCACX/NCOCX [64]). The DARR spectra were recorded with 2,048 direct point (spectral window 53.6 kHz/304 ppm) and 512 indirect points (spectral window 46.0 kHz/261 ppm). The mixing time and interscan delay were 50 ms and 3.0 s. The heteronuclear NCA correlation spectra were recorded with 176 scans, 1,536 points in the direct dimension (spectral window 64.1 kHz/300 ppm), 112 points in the indirect dimension (spectra window 7.9 kHz/92.1 ppm) and 3.2 s recycling delay. The 3D NCACX spectrum was recorded with 48 scans, 1.5 k points in the direct dimension (spectral window 64.1 kHz/300 ppm), and 80 and 60 points for 13C and 15 N indirect dimensions (13Cα spectral window 14.0 kHz/65.5 ppm, 15 N spectra window 7.9 kHz/92.1 ppm). The 3D NCOCX spectrum was recorded with 48 scans, 1,536 points in the direct dimension (spectral window 64.1 kHz/300 ppm), and 56 and 60 points for ^{13}C and ^{15}N indirect dimensions (13Cα spectral window 7.0 kHz/32.7 ppm, ^{15}N spectra window 7.9 kHz/92.1 ppm). The mixing time and interscan delay were 40 ms and 2.7 s for both NCACX and NCOCX experiments. The ^{13}C and ^{15}N chemical shifts were referenced as in previous works [39, 65]

The 2D ^{1}H-^{13}C INEPT-HETCOR was recorded with a refocused INEPT sequence with 224 scans, 2,048 points in the direct dimension (spectral window 53.6 kHz/304 ppm) and 112 points in the indirect dimension (7.9 kHz/11.3 ppm). WALZ decouplig at 2.5 kHz was applied during the ^{13}C detection.

All spectra were processed with zero-filling of the direct dimension to 4 k points and with a cosine apodization with sine bell shift of 2. Along the indirect dimensions, the 2D DARR spectra were zero-filled to 1 k points, the 2D NC correlation spectra to 512 points and the 3D NCC spectra to 128 points.

Results

The first remarkable feature of the sample, from the SSNMR-spectroscopic point of view, is that it contains both a rigid and a mobile part: the signals of the ^{13}C nuclei

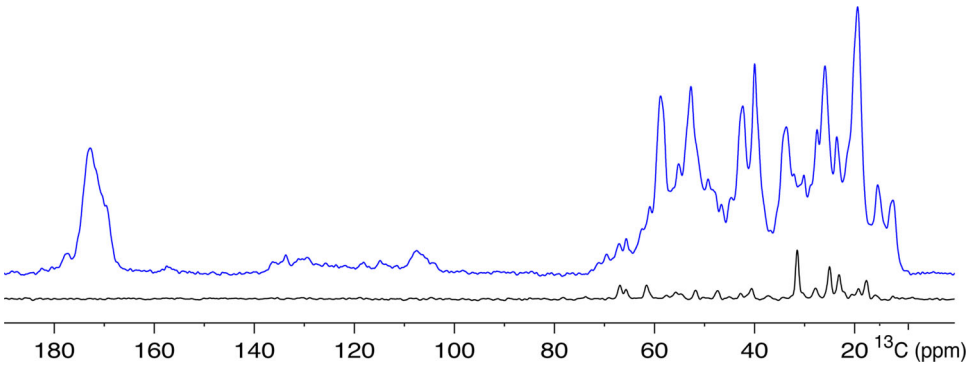

Fig. 1 Comparison of the 1D ^{1}H-^{13}C CP spectrum (128 scans, *blue*) and the ^{1}H-^{13}C INEPT spectrum (1,024 scans, *black*) of the SODΔIV–VII fibrils sample, recorded at 700 MHz. The MAS frequency was set to 14 kHz. For the CP spectrum a ^{1}H SWTPPM decoupling of 75 kHz was applied. For the INEPT spectrum, ^{1}H WALZ decoupling at 2.5 kHz was applied. NMR signals in the INEPT spectrum suggest the presence of a mobile component in SODΔIV–VII fibrils

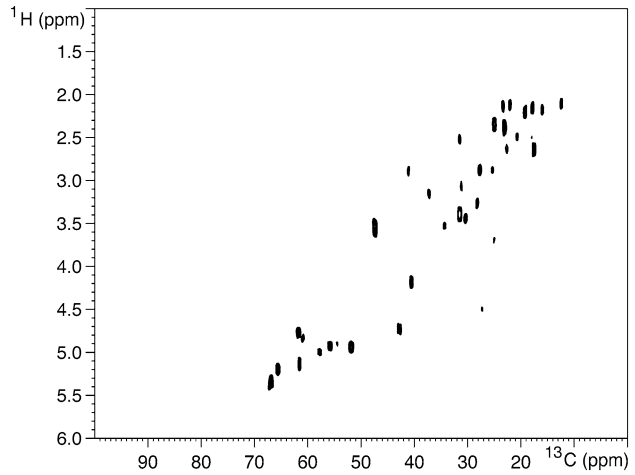

Fig. 2 ^{1}H-^{13}C INEPT-HETCOR spectrum recorded on the SODΔIV–VII fibrils sample. NMR signals in the spectrum suggest the presence of a mobile component in SODΔIV–VII fibrils. The MAS frequency was set to 14 kHz; ^{1}H WALZ decoupling at 2.5 kHz was applied

in the sample can be enhanced by cross-polarization (CP, [66]) as expected for being located in a solid but, at the same time, a different subset of signals can be observed in the INEPT spectrum (Figs. 1, 2) [67].

The observation of INEPT signals from a solid sample is possible only if there are free monomers in solution or if some regions of the protein experience a substantial mobility in the ns timescale. The number of peaks in the INEPT spectrum (and also in the 2D ^{1}H-^{13}C INEPT-HETCOR) is however rather small, suggesting that they originate from some residual mobility in an otherwise fully formed fibril rather than from a mixture of fully immobilized fibrils and free monomers. To prove that the signals present in the INEPT spectrum result from the mobile regions of fibrils rather than from free monomers, the same INEPT spectrum has been acquired on the monomeric apoSODΔIV–VII in solution. The latter displays a significantly larger number of peaks as expected for a protein of 110 residues (Figure S1). This behavior indicates that, despite the elimination of the loops, some regions of the fibrils are quite flexible.

The characterization of the CP-responsive, solid-part type was carried out with the usual toolbox of SSNMR. There are several aspects of the SSNMR spectra that are worth mentioning:

(a) the spectra show several more resonances than what it could be expected for a protein of 110 residues, in particular when some parts of the protein are mobile and absent from CP-based spectra;
(b) many spectral regions are even more crowded and less spread than those found in WT apoSOD1 protein in microcrystals (Fig. 3); collectively, points a and b indicate that the system is largely heterogeneous, suggesting a polymorphic arrangement of the fibrils, as it can be inferred also from previously reported results [28]; it should be noticed that even so the spectra obtained here are still of significantly better quality than those recorded on the oligomers or fibrils formed by full-length SOD1 protein.
(c) We found that CNC-type 3D experiments, requiring two double-CP steps, yield no signals. This may be due to the fact that the effective sample is partially compromised by the presence of multiple forms or possibly indicates that the sample suffers from dehydration.
(d) Some of the peaks are sequentially assignable or, at least, residue-specifically assignable (Table S1 and Figure S2).[1] This indicates that, along with the

[1] The ^{13}C and ^{15}N resonance assignments (code 19767) have been deposited to the Biological Magnetic Resonance Data Bank (http://www.bmrb.wisc.edu/).

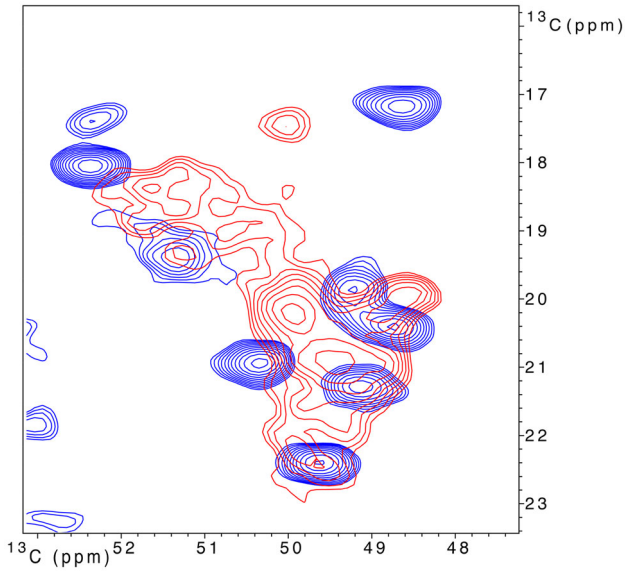

Fig. 3 Enlargement of the Alanine Ca–Cb region showing the lower spreading of the signals in the fibrillar aggregates of apoSODΔIV–VII (*red*) with respect to the crystalline WT apo protein (*blue*)

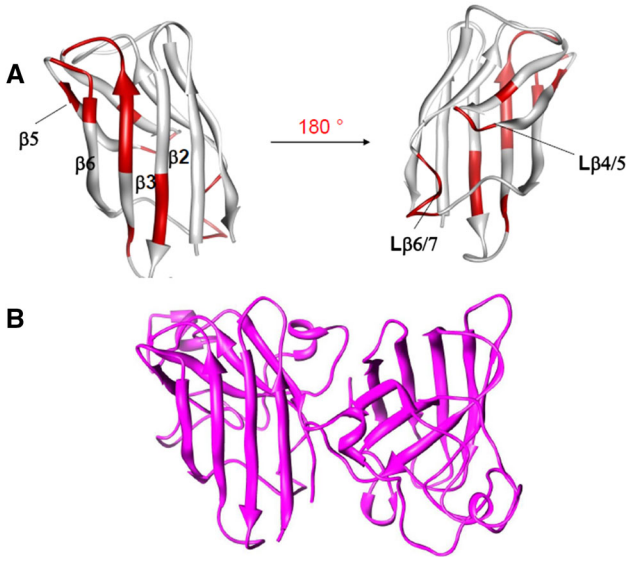

Fig. 4 **a** Mapping of the assigned residues onto the apoSODΔIV–VII X-ray structure (PDBID 4BCZ). **b** Solution structure of the wild-type apo SOD1 (PDBID:3ECU)

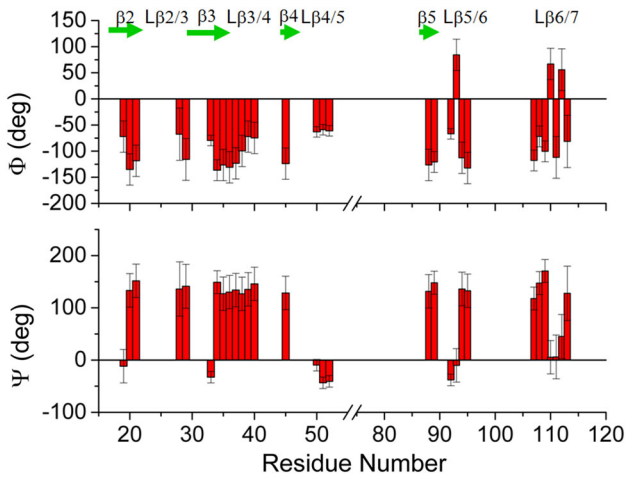

Fig. 5 Predicted backbone dihedral angles from PREDITOR [71] for the assigned residues. The secondary structure elements of the assigned residues as found in the apoSODΔIV–VII X-ray structure are shown at the *top*

heterogeneous component, a highly homogenous component is also present and could represent the fibrillar core. This resembles the recent report on a large prion fibrillar assemblies on which chemical shift assignment of the fibril core region can be achieved while the overall 2D spectra resolution is rather low [68]

We could identify and assign residue-specific spin systems for as many as 54 amino acids: out of these, we have site-specifically assigned 30 residues (Figure S1), for which it was possible to follow a sequential connectivity. The other 24 residue-specifically assigned spin systems were 9 Gly, 4 Thr/Ser, 4 Ala and 7 Asp/Asn.

The site-specifically assigned residues are located in β2 (residues 19–21 in the WT SOD1 numbering), β3 (33–36), β4 (45) and β5 (88–89) strands, and in the loops connecting β2–β3 (28–29), β3–β4 (37–40), β4–β5 (50–52), β5–β6 (92–95), β6–β7 (107–113). Of these, only the loop between β6 and β7 sits in the intersubunit region of the dimeric wild-type hSOD1 (Fig. 4). Chemical shifts of assigned residues can be correlated to backbone dihedral angles, which, in turn, are related to secondary structure elements (Fig. 5). The latter are predicted to be mainly beta strands, with the exception of scattered values for some residues located in the loop between β5 and β6 (Lβ5/6), which contains the first Gly-Ala-Gly tripeptide linker, and some residues at the C-terminus of Lβ6/7. The structural prediction reported in Fig. 5 shows that some of the residues with beta properties are found in loops Lβ2/3 and Lβ3/4. This occurs also in the monomeric WT apo protein as well as in microcrystalline samples of oxidized dimeric apo WT protein [34], in line with the presence of a low-populated state with increased order in these regions of loops as described in [69]. The structural prediction for fibrils in loops Lβ3/4 and Lβ6/7 differs from the secondary structure propensity reported for apoSODΔIV–VII in solution [58] as the latter shows a decreased beta tendency in both loop regions.

The structure of the mutant variant H43F, which lacks the dynamic motions of the β4/β5 sheet, characteristic for the WT protein could provide a clue to the structure of the excited state: the structure of H43F shows more continuous hydrogen bonding of the sheet than the distorted WT apoSOD1 [70].

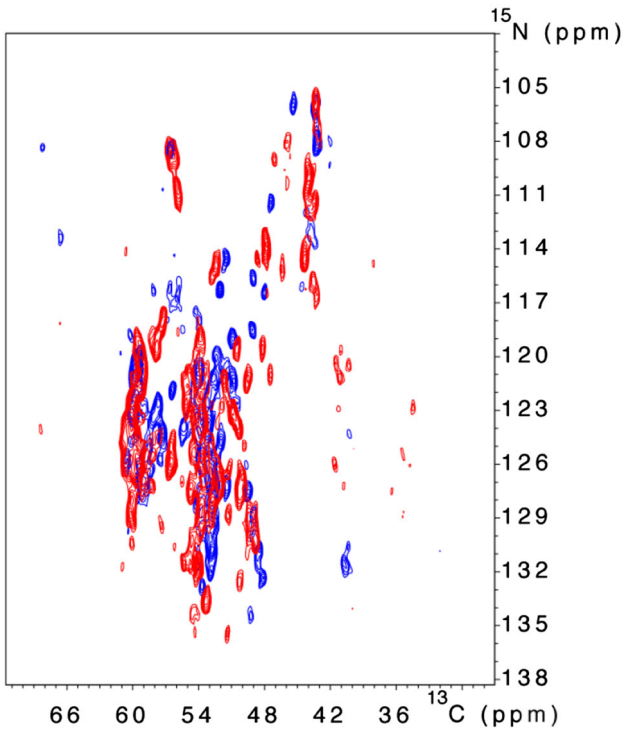

Fig. 6 Comparison between the NCA spectra of the fibrils obtained from the monomeric truncated mutant apoSODΔIV–VII (*red*) and those of the fibrils obtained from the WT apoSOD1 (*blue*)

Discussion and conclusions

SSNMR 2D spectra of apoSODΔIV–VII fibrils are overcrowded, with respect to the number of peaks expected for a protein of 110 residues. This is not surprising, even in this truncated variant of the protein, given that SOD1 fibrils are known to be polymorphic [28]. The construct we are characterizing contains two out of the three regions that are found to be not accessible to limited proteolysis [28], as well as the regions that were proposed to be the most important for fibrillization [36]. The NCA SSNMR spectrum of the present fibril sample obtained from the truncated apoSODΔIV–VII is comparable to a subset of the spectrum of the fibrils of the WT protein, although obtained in different experimental conditions. The spectrum of the WT protein is however more complex and more crowded (Fig. 6). We might therefore conclude that this truncated monomeric construct is a reasonable proxy for the final fibrillar species of the WT protein.

Despite the significant spectral crowding, we were able to track the sequential connectivity through 30 residues and have further identified 24 spin systems. It has been proposed based on proteolysis and mass spectrometry data that the fibrillation core in WT SOD1 and its mutants involves residues 1–63 [36]. Even if it cannot be excluded that each sequential connectivity may belong to different fibrillar states, as in the case of some Aβ polymorphs [39, 53, 72], most of the residues assigned by SSNMR and therefore present in an ordered conformation are present in the 1–63 stretch, thus confirming the observations reported in [36] that these residues are comprised in the fibrillar core.

The differences between the secondary structure elements predicted in the present fibrillar and those observed in the crystal structure of apoSODΔIV–VII, and in solution for the monomeric apoSODΔIV–VII, indicate that β3, which is located in the fibrillar nucleation site, is lengthened. Analysis of the urea dependence of the SOD1 fibrillation kinetics [35] led to the suggestion that a globally unfolded state might be the starting point for the fibrillation process, rather than the low-populated excited state. As globally unfolded SOD1 exposes several aggregation competent segments, each of which compete with one another in the fibril nucleation process, this precursor is expected to give rise to heterogeneous fibrillar morphology, consistent with the observations in this and previous studies. Such heterogeneity is further expected to be modulated by fluctuations in secondary structure propensity and diffuse long-range interactions in the denatured ensemble [70]. Coupled to the variation of sequence segments recruited into the fibrillar spine, there is also heterogeneity in the more flexible sequence regions looping out from the fibrillar surface: the results show clearly that only a fraction of the SOD1 backbone is fixed in the fibrillar structure whereas parts seem to remain disordered (Fig. 2). Interestingly, this could open up alternative therapeutic strategies—intervention need not only be limited to targeting of the precursors or the ordered fibrillar spine, but could also be achieved by targeting of the more amenable, disordered sequence regions decorating the fibrillar surface.

Acknowledgments The projects PRIN (2009FAKHZT_001) "Biologia strutturale meccanicistica: avanzamenti metodologici e biologici", BIO-NMR (contract no. 261863, NMR for Structural Biology, We-NMR (contract no. 261572, "A worldwide e-Infrastructure for NMR and structural biology") are acknowledged for funding. This work was also supported by Instruct, part of the European Strategy Forum on Research Infrastructures (ESFRI) and supported by national member subscriptions. Specifically, we thank the EU ESFRI Instruct Core Centre CERM–Italy.

References

1. Fowler DM, Koulov AV, Balch WE, Kelly JW (2007) Trends Biochem Sci 32:217–224
2. Ross CA, Poirier MA (2004) Nat Med 10:S10–S17
3. Luheshi LM, Crowther DC, Dobson CM (2008) Curr Opin Chem Biol 12:25–31
4. Rosen DR, Siddique T, Patterson D, Figlewicz DA, Sapp P, Hentati A, Donaldson D, Goto J, O'Regan J, Deng HX, Rahmani Z, Krizus A, McKenna-Yasek D, Cayabyab A, Gatson SM, Berger R, Tanzi RE, Halperin JJ, Herzfeldt B, Van der Bergh R, Hung W-Y, Bird, Deng G, Mulder DW, Smyth C, Laing NG,

Soriano E, Pericak-Vance MA, Haines J, Rouleau GA, Gusella JS, Horvitz HR, Brown RH Jr (1993) Nature 362:59–62
5. Borchelt DR, Lee MK, Slunt HS, Guarnieri M, Xu ZS, Wong PC, Brown RH, Price DL, Sisodia SS, Cleveland DW (1994) Proc Natl Acad Sci USA 91:8292–8296
6. Deng HX, Hentati A, Tainer JA, Lqbal Z, Cyabyab A, Hang W-Y, Getzoff ED, Hu P, Herzfeldt B, Roos RP, Warner C, Deng G, Soriano E, Smyth C, Parge HE, Ahmed A, Roses AD, Hallewell RA, Pericak-Vance MA, Siddique T (1993) Science 261:1047–1051
7. Blokhuis AM, Groen EJN, Koppers M, Van den Berg L, Pasterkamp RJ (2013) Acta Neuropathol 125:777–794
8. Sheng Y, Chattopadhyay M, Whitelegge JP, Valentine JS (2012) Curr Top Med Chem 12:2560–2572
9. Forsberg K, Jonsson PA, Andersen PM, Bergemalm D, Graffmo KS, Hultdin M, Jacobsson J, Rosquist R, Marklund SL, Brannstrom T (2010) PLoS ONE 5:e11552
10. Zetterström P, Andersen PM, Brannstrom T, Marklund SL (2011) J Neurochem 117:91–99
11. Shaw BF, Lelie HL, Durazo A, Nersissian AM, Xu G, Chan PK, Gralla EB, Tiwari A, Hayward LJ, Borchelt DR, Valentine JS, Whitelegge JP (2008) J Biol Chem 283:8340–8350
12. Kato S, Hayashi H, Nakashima K, Nanba E, Kato M, Hirano A, Nakano I, Asayama K, Ohama E (1997) Am J Pathol 151: 611–620
13. Banci L, Bertini I, Girotto S, Martinelli M, Vieru M, Whitelegge J, Durazo A, Valentine JS (2007) Proc Natl Acad Sci USA 104:11263–11267
14. Bosco DA, Morfini G, Karabacak NM, Song Y, Gros-Louis F, Pasinelli P, Goolsby H, Fontaine BA, Lemay N, McKenna-Yasek D, Frosch MP, Agar JN, Julien JP, Brady ST, Brown RH Jr (2010) Nat Neurosci 13:1396–1403
15. Bruijn LI, Houseweart MK, Kato S, Anderson KL, Anderson SD, Ohama E, Reaume AG, Scott RW, Cleveland DW (1998) Science 281:1851–1854
16. Pasinelli P, Belford ME, Lennon N, Bacskai BJ, Hyman BT, Trotti D, Brown RH Jr (2004) Neuron 43:19–30
17. Cozzolino M, Pesaresi MG, Amori I, Crosio C, Ferri A, Nencini M, Carri MT (2009) Antioxid Redox Signal 11:1547–1548
18. Hayward LJ, Rodriguez JA, Kim JW, Tiwari A, Goto JJ, Cabelli DE, Valentine JS, Brown RHJ (2002) J Biol Chem 277(18): 15923–15931
19. Rodriguez JA, Valentine JS, Eggers DK, Roe JA, Tiwari A, Brown RHJ, Hayward LJ (2002) J Biol Chem 277:15932–15937
20. Roe JA, Butler A, Scholler DM, Valentine JS, Marky L, Breslauer KJ (1988) Biochemistry 27:950–958
21. Banci L, Bertini I, D'Amelio N, Libralesso E, Turano P, Valentine JS (2007) Biochemistry 46:9953–9962
22. Chattopadhyay M, Durazo A, Sohn SH, Strong CD, Gralla EB, Whitelegge JP, Valentine JS (2008) Proc Natl Acad Sci USA 105:18663–18668
23. Furukawa Y, Kaneko K, Yamanaka K, O'Halloran TV, Nukina N (2008) J Biol Chem 283:24167–24176
24. Banci L, Bertini I, Boca M, Girotto S, Martinelli M, Valentine JS, Vieru M (2008) PLoS ONE 3:e1677
25. Nordlund A, Leinartaite L, Saraboji K, Aisenbrey C, Grobner G, Zetterstrom P, Danielsson J, Logan DT, Oliveberg M (2009) Proc Natl Acad Sci USA 106:9667–9672
26. Karch CM, Borchelt DR (2010) Arch Biochem Biophys 503: 175–182
27. Nordlund A, Oliveberg M (2006) Proc Natl Acad Sci USA 103:10218–10223
28. Furukawa Y, Kaneko K, Yamanaka K, Nukina N (2010) J Biol Chem 285:22221–22231
29. Banci L, Bertini I, Boca M, Calderone V, Cantini F, Girotto S, Vieru M (2009) Proc Natl Acad Sci USA 106:6980–6985
30. Doucette PA, Whitson LJ, Cao X, Schirf V, Demeler B, Valentine JS, Hansen JC, Hart PJ (2004) J Biol Chem 279: 54558–54566
31. Arnesano F, Banci L, Bertini I, Martinelli M, Furukawa Y, O'Halloran TV (2004) J Biol Chem 279:47998–48003
32. Lindberg MJ, Normark J, Holmgren A, Oliveberg M (2004) Proc Natl Acad Sci USA 101:15893–15898
33. Ding F, Furukawa Y, Nukina N, Dokholyan NV (2012) J Mol Biol 421:548–560
34. Banci L, Bertini I, Blazevits O, Cantini F, Lelli M, Luchinat C, Mao J, Vieru M (2011) J Am Chem Soc 133:345–349
35. Lang L, Kurnik M, Danielsson J, Oliveberg M (2012) Proc Natl Acad Sci USA 109:17868–17873
36. Chan PK, Chattopadhyay M, Sharma S, Souda P, Gralla EB, Borchelt DR, Whitelegge JP, Valentine JS (2013) Proc Natl Acad Sci USA 110:10934–10939
37. Tang M, Comellas G, Rienstra CM (2013) Acc Chem Res 46:2080–2088
38. Habenstein B, Bousset L, Sourigues Y, Kabani M, Loquet A, Meier BH, Melki R, Böckmann A (2012) Angew Chem Int Ed Engl 51:7963–7966
39. Bertini I, Gonnelli L, Luchinat C, Mao J, Nesi A (2011) J Am Chem Soc 133:16013–16022
40. Sun SJ, Siglin A, Williams JC, Polenova T (2009) J Am Chem Soc 131:10113–10126
41. Byeon I-JL, Hou G, Han Y, Suiter CL, Ahn J, Jung J, Byeon C-H, Gronenborn AM, Polenova T (2012) JACS 134:6455–6466
42. Loquet A, Sgourakis NG, Gupta R, Giller K, Riedel D, Goosmann C, Griesinger C, Kolbe M, Baker D, Becker S, Lange A (2012) Nature 486:276–279
43. Loquet A, Habenstein B, Lange A (2013) Acc Chem Res 46:2070–2079
44. Bertini I, Gallo G, Korsak M, Luchinat C, Mao J, Ravera E (2013) ChemBioChem 14:1891–1897
45. Petkova AT, Ishii Y, Balbach JJ, Antzutkin ON, Leapman RD, Delaglio F, Tycko R (2002) Proc Natl Acad Sci USA 99:16742–16747
46. Tycko R, Ishii Y (2003) J Am Chem Soc 125:6606–6607
47. Chimon S, Shaibat MA, Jones CR, Calero DC, Aizezi B, Ishii Y (2007) Nat Struct Mol Biol 14:1157–1164
48. Debelouchina GT, Platt GW, Bayro MJ, Radford SE, Griffin RG (2010) J Am Chem Soc 132:10414–10423
49. Van der Wel PCA, Lewandowski JR, Griffin RG (2010) Biochemistry 49:9457–9469
50. Bayro MJ, Maly T, Birkett NR, MacPhee CE, Dobson CM, Griffin RG (2010) Biochemistry 49:7474–7484
51. Lopez del Amo JM, Fink U, Dasari M, Grelle G, Wanker EE, Bieschke J, Reif B (2012) J Mol Biol 421:517–524
52. Bieschke J, Herbst M, Wiglenda T, Friedrich RP, Boeddrich A, Schiele F, Kleckers D, Lopez del Amo JM, Grüning BA, Wang Q, Schmidt MR, Lurz R, Anwyl R, Schnoegl S, Fandrich M, Frank RF, Reif B, Günther S, Walsh DM, Wanker EE (2012) Nat Chem Biol 8:93–101
53. Lopez del Amo JM, Schmidt M, Fink U, Dasari M, Fändrich M, Reif B (2012) Angew Chem Int Ed Engl 51:6136–6139
54. Goobes G, Goobes R, Schueler-Furman O, Baker D, Stayton PS, Drobny GP (2006) Proc Natl Acad Sci USA 103:16083–16088
55. Goobes G, Stayton PS, Drobny GP (2007) Progr NMR Spectrosc 50:71–85
56. Roerich A, Drobny GP (2013) Acc Chem Res 46:2136–2144
57. Fragai M, Luchinat C, Martelli T, Ravera E, Sagi I, Solomonov I, Udi Y (2014) Chem Commun (Camb.) 50(4):421–423
58. Danielsson J, Kurnik M, Lang L, Oliveberg M (2011) J Biol Chem 286:33070–33083
59. Petkova AT, Yau WM, Tycko R (2006) Biochemistry 45: 498–512

60. Fandrich M, Schmidt M, Grigorieff N (2011) Trends Biochem Sci 36:338–345
61. Takegoshi K, Nakamura S, Terao T (1999) Chem Phys Lett 307:295–302
62. Baldus M, Petkova AT, Herzfeld J, Griffin RG (1998) Mol Phys 95:1197–1207
63. Loening NM, Bjerring M, Nielsen NC, Oschkinat H (2012) J Magn Reson 214:81–90
64. Pauli J, Baldus M, van Rossum B, de Groot H, Oschkinat H (2001) ChemBioChem 2:272–281
65. Igumenova TI, Wand AJ, McDermott AE (2004) J Am Chem Soc 126:5323–5331
66. Pines A, Gibby MG, Waugh JS (1972) J Chem Phys 56: 1776–1777
67. Morris GA, Freeman R (1979) J Am Chem Soc 101:760–762
68. Luckgei N, Schütz AK, Bousset L, Habenstein B, Sourigues Y, Gardiennet C, Meier BH, Melki R, Böckmann A (2013) Angew Chem Int Ed. doi:10.1002/anie.201304699
69. Teilum K, Smith MH, Schulz E, Christensen LC, Solomentsev G, Oliveberg M, Akke M (2009) Proc Natl Acad Sci USA 106:18273–18278
70. Danielsson J, Awad W, Saraboji K, Kurnik M, Lang L, Leinartaite L, Marklund SL, Logan DT, Oliveberg M (2013) Proc Natl Acad Sci USA 110:3829–3834
71. Berjanskii MV, Neal S, Wishart DS (2006) Nucleic Acids Res 34:W63–W69
72. Qiang W, Yau W-M, Tycko R (2011) J Am Chem Soc 133: 4018–4029